JOURNAL OF GEOPHYSICAL RESEARCH, VOL. 103, NO. D24, PAGES 31,695–31,707, DECEMBER 27, 1998

# Variability of water vapor in the tropical upper troposphere as measured by the Microwave Limb Sounder on UARS

H.L. Clark and R.S. Harwood

Department of Meteorology, University of Edinburgh, Scotland, United Kingdom

P.W. Mote[1]

Northwest Research Associates, Bellevue, Washington

W.G. Read

Jet Propulsion Laboratory, California Institute of Technology, Pasadena

**Abstract.** The Microwave Limb Sounder (MLS), an instrument on the Upper Atmosphere Research Satellite (UARS), measures water vapor in the upper troposphere, with best sensitivity at the standard UARS level at 215 hPa. In this paper, we analyze the MLS observations with a view to characterizing the temporal and zonal variations of upper tropospheric water vapor between 20°N and 20°S. Time series of water vapor throughout the tropics show a strong annual cycle with maximum amplitude at 20°N and 90°E. An intraseasonal cycle with a period of 30–85 days is evident over the Western Pacific at latitudes from 10°N to 20°S. The cycle is associated with eastward propagating disturbances of zonal wavenumbers 1–2, suggesting that this intraseasonal cycle is related to the Madden-Julian oscillation.

## 1. Introduction

Water vapor is a significant absorber and emitter of infrared radiation and is the most dominant greenhouse gas [e.g., *Houghton et al.,* 1990; *Jones and Mitchell,* 1991]. The response of the climate to increases in anthropogenic greenhouse gases depends upon the water vapor feedback, which is generally believed to be positive; increased global temperatures lead to an increase in water vapor, in turn contributing to further warming. *Lindzen* [1990] suggested that increased global temperatures and consequent increased convection may lead to a drying of the upper troposphere through subsidence, which could offset some warming. Some debate still surrounds this idea as more recent papers suggest [e.g., *Chou,* 1994; *Soden,* 1997; *Spencer and Braswell,* 1997] and the primary reason for the continuing uncertainty is the lack of adequate global water vapor measurements in the upper troposphere.

Historically, measurements of the water vapor field have relied upon radiosonde profiles; the accuracy and spatial extent of which are limited [e.g., *Elliot and Gaffen,* 1991; *Soden and Lanzante,* 1996]. Radiosonde profiles are confined largely to northern hemisphere landmasses with the result that the water vapor field in the upper troposphere of the tropical region has been poorly observed. Satellites provide a better way to achieve greater spatial and temporal coverage. The Microwave Limb Sounder (MLS) on the Upper Atmosphere Research Satellite (UARS) is sensitive to water vapor in the upper troposphere. With a 3 km field of view in the vertical, it has greater vertical resolution than that of infrared instruments such as Meteosat [*Schmetz and Turpienen,* 1988], the U.S. Geostationary Operational Environmental Satellite (GOES) [*Soden and Bretherton,* 1993], and the TIROS Operational Vertical Sounder [*Salathé and Chesters,* 1995], which are sensitive to water vapor in a broad layer of the upper troposphere $\sim$ 300hPa thick. The MLS measurement of upper tropospheric humidity (UTH) is relatively insensitive to cirrus clouds, giving it additional advantages over infrared techniques. The temporal resolution of MLS is better than that of solar occultation instruments such as the Stratospheric Aerosol and Gas Experiment 2 (SAGE II) from which measurements are limited to $\sim$ 30 per day. For several years, MLS has provided daily coverage of the tropical region since its launch in September 1991.

The MLS water vapor data reveal synoptic-scale features and detrainment streams extending from tropical convective regions [*Read et al.,* 1995], as well as the gross annual variations of the zonal mean [*Elson et al.,* 1996]. In the tropics, *Newell et al.* [1996] have shown that the observed distribution of water vapor is consistent with the Walker circulation, and *Newell et al.* [1997] have shown that upper tropospheric

[1]Also at Joint Institute for the Study of the Atmosphere and Ocean, University of Washington, Seattle



Paper number 98JD02702.
0148-0227/98/98JD-02702$09.00

water vapor is closely related to sea surface temperature variations in the eastern Pacific. In this paper, the MLS measurement will be used to examine the temporal and zonal variability of upper tropospheric water vapor in the tropical region and to account for the observed variability by relating it to known processes.

## 2. Data

UARS is in an almost circular orbit at an altitude of 585 km and an inclination of 57° to the equator [*Reber*, 1993]. It makes ~ 14 orbits each day with adjacent orbits being separated by ~ 2670 km at the equator, thereby allowing a zonal mean and six wavenumbers to be resolved. MLS makes a limb scan perpendicular to the orbit path at tangent heights from 90 km to the surface. Each scan takes 65.5 s and consists of a profile of measurements which are usually retrieved onto 15 pressure levels. MLS provides a 3 km field of view in the vertical. Latitudinal coverage changes from between 80°N and 34°S to 34°N and 80°S because the satellite performs a yaw maneuver about every 36 days, but the tropical region is observed daily, enabling a nearly continuous time series to be constructed. The MLS instrument is described in more detail by *Barath et al.* [1993], and the measurement technique is described by *Waters* [1993].

The 205 GHz channel on MLS is principally used to measure chlorine monoxide but it is sensitive to water vapor in the upper troposphere when concentrations are in the range of 100 to 300 ppmv [*Read et al.*, 1995]. The best sensitivity occurs when the water vapor concentration is about 150 ppmv; of the standard UARS pressure levels, it is at 215 hPa (~ 12 km at low latitudes and ~ 7 km at high latitudes) that this concentration most often occurs. We therefore focus our study on the 215 hPa level.

Retrievals in the upper troposphere may be affected by thick cirrus clouds. In the tropical region between 6 and 12 km, the retrievals are not significantly affected, but at latitudes poleward 40°, a significant fraction of the measured radiances may come from scattering by cirrus clouds [*Bond*, 1996]. Ice crystals in cirrus clouds at a concentration of 0.1 g $m^{-3}$ over a horizontal distance of 120 km could contribute to 20% of the absorption coefficient at 215 hPa but will usually be less, and at concentrations less than 0.01 g $m^{-3}$ the effect is negligible [*Read et al.*, 1995].

The data are derived from the initial MLS UTH retrieval as described by *Read et al.* [1995]. A new and improved MLS UTH retrieval has recently been developed, which among other features has a formal error estimation calculation and has been compared with Vaisala thin-film capacitive radiosonde measurements. Comparisons with the newer product show the current analyzed product at 215 hPa, which is used in this paper, to be biased high by 50-60 ppmv (everywhere) and to have a precision of 5 ppmv.

Footprints were interpolated onto points spaced every 5° in longitude around latitude circles at 20°N, 10°N, the equator, 10°S, and 20°S. Footprints that fell within a given "search radius" of these points were given a distance weighting based upon the regression retrieval and space-time interpolation method used by *Jackson et al.* [1990]. A search radius of 2150 km was used with a scaling distance of 1000 km so that footprints 1000 km away from the given grid point have a relative weighting of 1/e whereas any that fall directly on the grid point have a relative weighting of 1. Zonal and meridional winds and vertical velocity were taken from the European Centre for Medium Range Weather Forecast's (ECMWF) initialized reanalysis data, which are gridded with a 2.5° by 2.5° resolution on the standard pressure levels.

## 3. Results

Whereas *Elson et al.* [1996] focused on the variability of zonal mean water vapor in latitude-time plots, we focus on the variability of zonal cross sections in longitude-time plots. First, we discuss the variability at low frequencies that is associated with the annual cycle. Next, we discuss intraseasonal variability and the connection between water vapor and meteorological fields.

To create longitude-time plots, the MLS footprints were first interpolated onto grid points as described in section 2. Data gaps were then filled in time using a Kalman filter. Most data gaps are of only 1 day, but a gap of ~ 2 weeks occurred in June 1992. The resulting longitude-time plots for the time period from December 1, 1991, to May 3, 1993, are shown in Plate 1, with the five regions showing the five latitude bins between 20°N and 20°S. Gaps longer than 3 days have been masked.

### 3.1. The Annual Cycle

In Plate 1 and particularly in Plates 1a, 1b, 1d, and 1e, an annual cycle in mixing ratio is apparent. Mixing ratios are high in local summer over continents when convection is strong and low in local winter when convection is weaker.

The northern hemisphere latitudes, 20°N and 10°N, are shown in Plates 1a and 1b respectively. The highest water vapor mixing ratios occur between 50°E and 120°E over the Indian Ocean and SE Asia from May to September when convection is strong. The annual cycle was isolated by least squares fitting to a sine wave. It is most pronounced in the region influenced by the Indian monsoon. At 20°N and 90°E, over the Bay of Bengal, it accounts for 80% of the variance in water vapor. Local maxima in the annual cycle occur just west of Panama as *Newell et al.* [1997] have noted, and minima over the cold eastern Pacific and Atlantic Oceans.

At the equator (Plate 1c), the range of mixing ratios is smaller than at the other tropical latitudes. The smaller range is probably because the Intertropical Convergence Zone (ITCZ) is rarely situated at the equator itself [*Philander et al.*, 1996]. The maximum mixing ratios are located over the Indian Ocean and Indonesia. The minimum mixing ratios occur over the eastern Pacific and are subject to an east-west migration on annual timescales, resulting in lower values extending further west in June-August and further east from November to January. As noted by *Newell et al.* [1997], the amplitude of the annual cycle, like the range, is smallest at the equator, and probably for the same reason. At the equa-

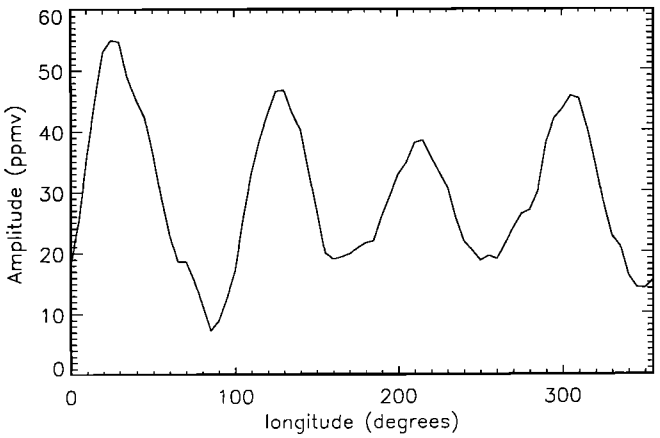


**Figure 1.** Amplitude of the annual cycle in water vapor mixing ratio (ppmv) at 10°S and 215 hPa.

tor, it exhibits its maximum amplitude at 90°W, off the coast of South America, where it accounts for 53% of the variance. *Newell et al.* [1997] showed that water vapor variations in the region 80°-90°W and 0°-10°S are related to variations in sea surface temperature (SST) caused by El Niño and also to anomalous changes in SST; the latter account for ~56% of the water vapor variance.

In the southern hemisphere, Plates 1d and 1e, mixing ratios are greater over Indonesia and South America during summer and lower over the eastern Pacific in winter. In the longitude-time section (Plate 1d), strong annual cycles can be seen over the African continent and South America. Figure 1 shows the variation of the amplitude of the annual cycle with longitude at 10°S and reveals further local maxima over Indonesia and the mid-Pacific. The influence of the cold eastern Pacific in suppressing convection and leading to a drier upper troposphere and of the warm western Pacific leading to a moister upper troposphere is evident in Plate 1d. This constitutes the Walker circulation with rising air in the west and subsiding air in the east. The influence of the Walker circulation on upper tropospheric water vapor from MLS has been noted by *Newell et al.* [1996] in two short periods of data from September 17 to October 22, 1991, and February 7 to March 14, 1994. Here, the presence of the Walker circulation can be seen to be a more persistent feature. Mixing ratios over the western Pacific show east-west migration similar to that at the equator, with low humidity found further west during winter, when the ocean is colder. Eastward moving features during the summer months originate over the warm Indian Ocean and are quickly terminated once they reach the eastern Pacific. These have a higher frequency than the annual cycle and are investigated by analyzing the time series with a focus on intraseasonal timescales.

### 3.2. Intraseasonal Variability

One of the main modes of variability in the tropics is the Madden-Julian oscillation (MJO) [*Madden and Julian,* 1971]. The MJO comprises large-scale circulation anomalies associated with convective anomalies which propagate eastward at 3-6 m $s^{-1}$. The dynamical signal of MJO, in zonal wind and surface pressure, has a period of 30-60 days and can be detected across the tropics. The convective signal has a broader range of 30-95 days [e.g., *Kiladis and Weickmann,* 1992; *Salby and Hendon,* 1994] and is strongest in the Indian Ocean and western Pacific.

Eastward moving moist features are apparent in the water vapor fields (Plate 1) and are most prominent at 10°S in southern summer. The moist anomalies at 10°S cover longitudes from 90°E to 245°E (115°W). One such feature begins at 105°E and travels to 190°E in ~22 days, thus moving with a speed of ~5 m $s^{-1}$. At the equator during southern summer, there are eastward moving features similar to those at 10°S, but they are less intense; during southern winter, eastward propagation is less common. Similar propagation of moist anomalies occurs at 10°N in northern summer with a more limited longitudinal extent, being confined mostly to the Indian Ocean. There is also evidence for the eastward movement of dry features between 130° and 280°E in northern hemisphere winter at 10° and 20°N (Plates 1a and 1b). In this section, the eastward moving moist features and their relationship to the MJO will be discussed.

The periodicity of the disturbances at a fixed longitude may be investigated from the power spectrum or from the lag correlogram. For a data set like that in Plate 1, the lag correlogram has some advantages, as it is insensitive to change of phase in the waves from one winter to the next and to whether the wave period is a proper harmonic of the length of the data set. Furthermore, it can reveal some information even when the waves exist for little more than one period.

Figure 2 shows the lag correlogram for 160°E and 10°S based on the 520 days of data used for Plate 1. Here, 160°E is illustrated as the longitude which exhibits the greatest intraseasonal variability. The annual cycle and low-frequency variability was removed from each longitude using a 150 day Butterworth filter. Also shown is the red noise background spectrum computed from lag-one autocorrelation [*Gilman et al.,* 1963] and the 95% confidence limits. The data have anticorrelation less than −0.2, at lags of 20–35 days, well below the red spectrum and significant at the 95% level. This is suggestive of waves of period 40–70 days, an interpretation supported by the existence of positive correlations at lags of 40–70 days. Inspection of Plate 1 suggests that these correlations arise from features which are only apparent in the southern summer months. Only slightly over one cycle is apparent in each year and so very high correlations cannot be expected. Moreover the magnitude of the correlation at the wave period will be necessarily less than that at the half period. By cross-correlating the time series at each longitude with the time series at 160°E using different lags, the estimated propagation speed was confirmed to be 4-5 m $s^{-1}$.

Figure 3 shows how the power at each frequency varies with longitude for 10°S. The strongest signal corresponds to a frequency of 0.014 $days^{-1}$ or a period of 70 days and falls within the frequency range associated with the convective signal of the MJO. The power spectrum was tested for significance at 95% by computing the signal to red noise ratio at each longitude and comparing it with the chi-squared distribution following the method of *Gilman et al.* [1963].

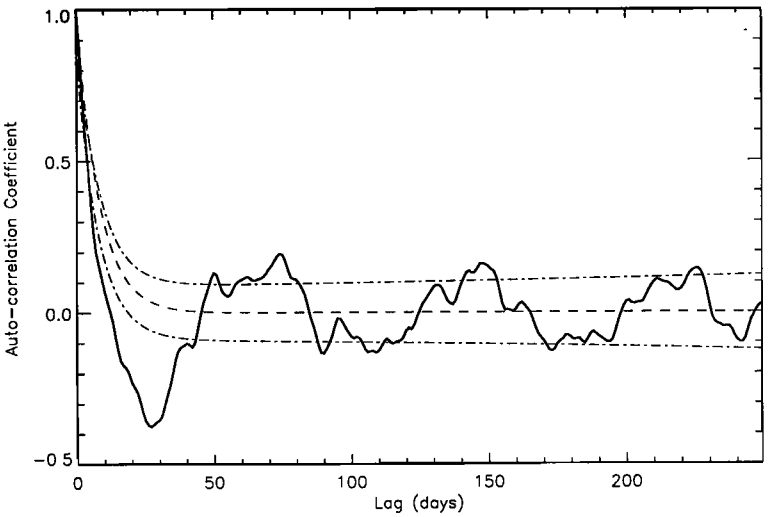


**Figure 2.** Auto-correlation of the time series of 215 hPa water vapor mixing ratios at 160°E and 10°S (solid line), red noise (dashed line), and 95% confidence limits (dash-dotted lines).

At 70 days and 160°E, values greater than 112ppm $^2$ are significant. The signal is confined in longitude from 140° to 180°E. This area, over the western Pacific, has been shown to exhibit strong intraseasonal variability in outgoing longwave radiation (OLR) which is often used to infer deep convection. *Salby and Hendon* [1994] examined 11 years of OLR data from the advanced very high resolution radiometer (AVHRR) and found that intraseasonal behavior was coincident with centers of climatological convection and warm sea surface temperature, with maxima over the Indian Ocean and western Pacific and secondary maxima over the eastern Pacific, Africa, and South America. They noted that most of the intraseasonal variance occurred over the Indian Ocean. This contrasts with the signal in water vapor which is dominant over the western Pacific. The absence of a signal in the water vapor field over the Indian Ocean may indicate that convective moistening is not reaching the 215 hPa level.

In order to focus on the intraseasonal frequency range characteristic both of the MJO and of the eastward moving disturbances seen in Plate 1, we filtered the water vapor data with a 30–85 day Butterworth band-pass filter similar to that used previously in studies of OLR [e.g., *Salby and Hendon,* 1994; *Zhang and Hendon,* 1997]. When applied to 520 days of data at 10°S and 160°E, the 30–85 day filter band accounted for 35% of the total power compared with 19% for the annual cycle. Mixing ratios in this band vary by

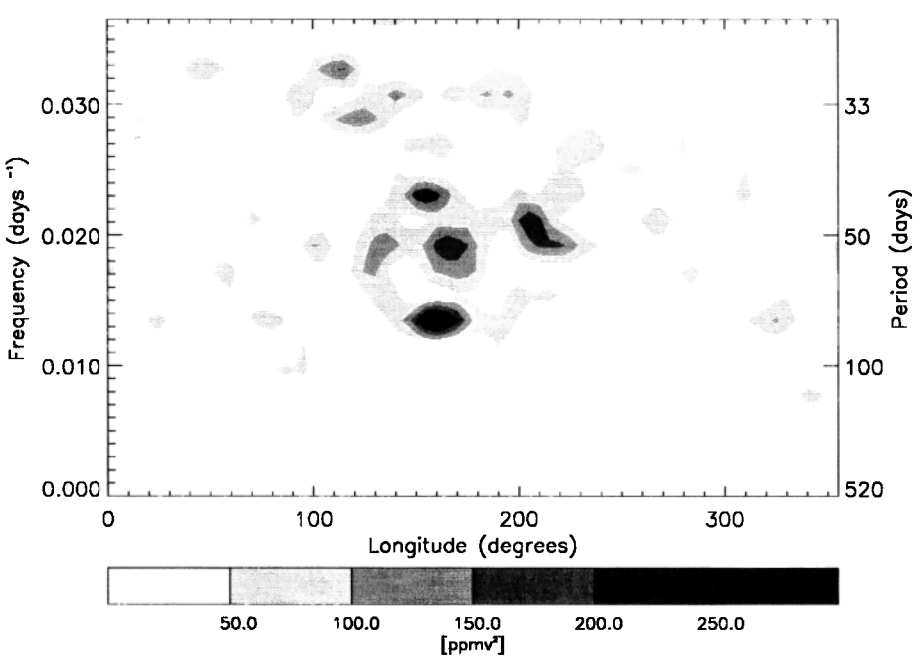


**Figure 3.** Power spectrum, as a function of longitude and frequency, of deseasonalized water vapor at 215 hPa. Contour intervals are 50 ppmv$^2$.

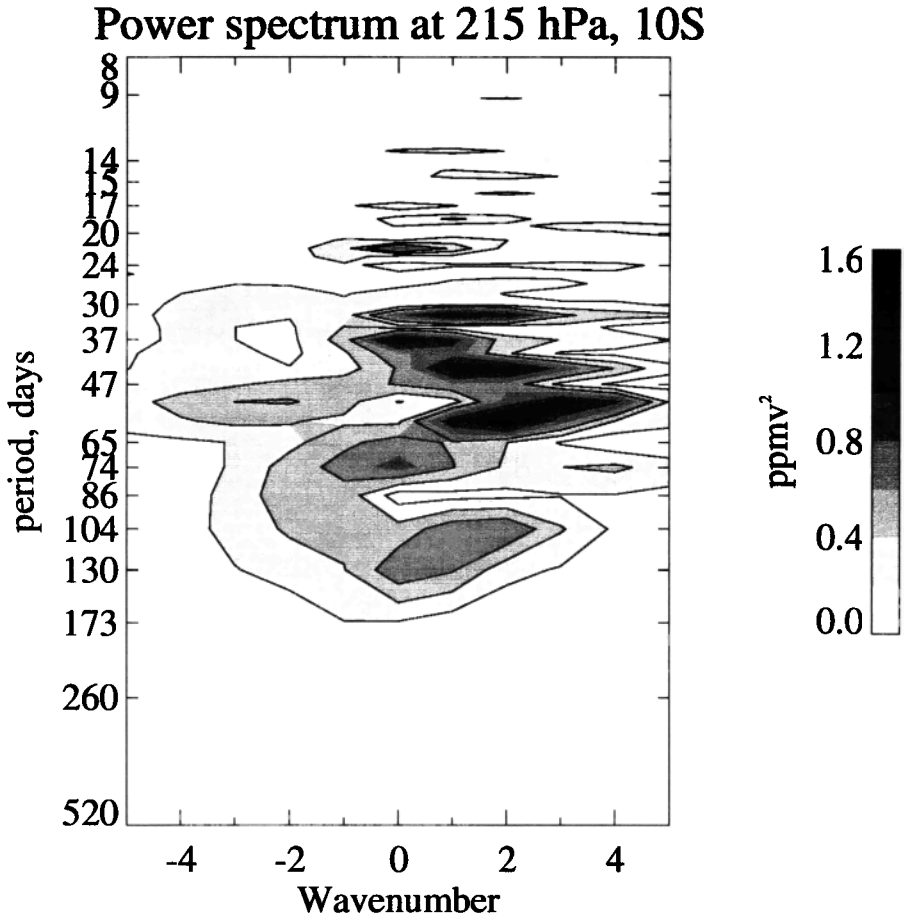


**Figure 4.** Power spectrum, as a function of wavenumber and frequency, of de-seasonalized water vapor at 215 hPa and 10°S.

± 60 ppmv. At the equator, intraseasonal activity occurring in the 30–85 day band accounts for 35% less power than at 10°S.

At 10°S the water vapor anomalies, consistent with the OLR signal [*Salby and Hendon*, 1994], possess a strong seasonality that is apparent in the longitude-time section (Plate 1d). The eastward propagating anomalies are strong when the ITCZ is near the latitude in question (local summer) but virtually absent when the ITCZ is not (local winter). When the eastward propagating anomalies are strong (December 1991 to March 1992), intraseasonal variability accounts for as much as 63% of the total variance, but, when they are weak (August–November 1992), intraseasonal variability only accounts for 7% of the total variance.

Further insights about the nature of the intraseasonal variability come from a wavenumber-frequency spectral analysis. The low-frequency variability was removed from 520 days of data using the 150 day band-pass filter as before, and the filtered data have been regressed against zonal and temporal harmonics of the form $\cos(kx - \omega t)$ to identify the power at discrete wavenumbers $k$ and frequencies $\omega$. Figure 4 shows the results of this analysis. There is very little power at the lowest frequencies, owing to the filtering; most power is concentrated in positive (eastward) wavenumbers 1–3 with periods from 30 to 60 days. Modes at $k = 0$ have a small share of the power, mostly at 37 and 74 days and represent a zonally symmetric mode. Because the zonal structure and frequency of the water vapor anomalies are similar to those usually identified with the convective component of the MJO (e.g., OLR), we tentatively identify these anomalies with the MJO.

To separate the modes of variability suggested by Figure 4, we calculate extended empirical orthogonal functions (EEOFs) [*Weare and Nasstrom*, 1982, *Wang et al.*, 1995]. Their more common cousins, empirical orthogonal functions (EOFs) , identify coherent variations by finding eigenvectors of the (symmetric) covariance matrix and ranking these eigenvectors in descending order of variance explained. For the longitude-time array of water vapor at 10°S, the covariance matrix for ordinary EOFs would be formed by summing (in time) the covariance $q_i(t)q_j(t)$ of water vapor $q_i(t)$ at every combination of longitudinal grid points. The EOFs would be one-dimensional functions of longitude and would yield a clearer picture of zonally coherent variations. Extended EOFs are found by calculating covariance of water vapor at each grid point not just with water vapor at other grid points but also at different lag times $l$, i.e., $q_{i,l}$, where the lag varies in this case between −60 and +60 days at 5

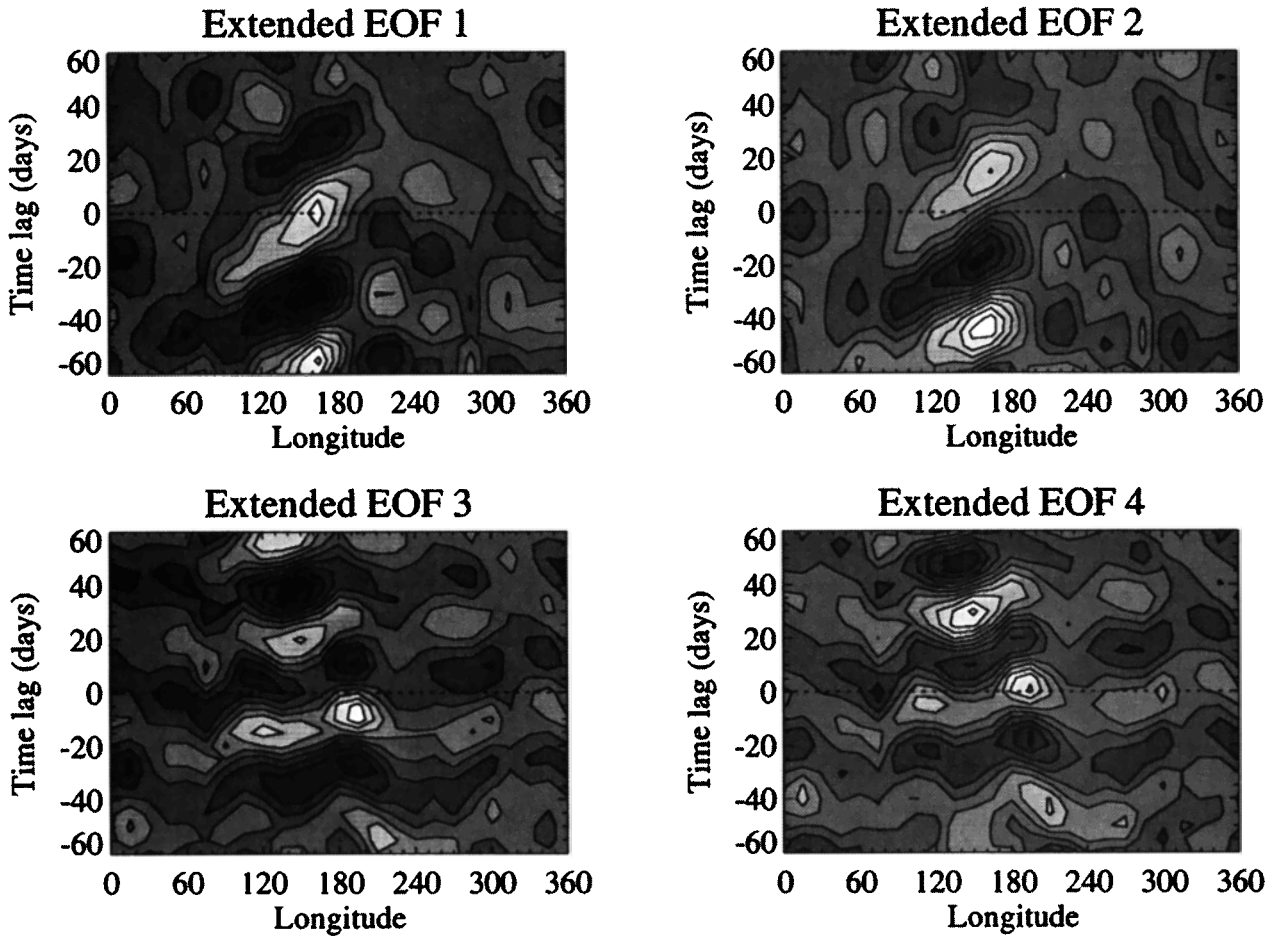


**Figure 5.** Spatiotemporal structure of the first four extended EOFs of deseasonalized water vapor at 215 hPa and 10°S.

day intervals. EEOF analysis yields a clearer picture of zonally and temporally coherent variations.

The first four EEOFs are shown in Figure 5. EEOFs (and EOFs) sometimes occur in conjugate pairs, identified by the closeness of their eigenvalues, by their associated time series which are in quadrature and by their spatiotemporal structure which is also in quadrature. The significance of conjugate pairs is that they describe a quasi-periodic oscillation of some sort. The first pair of EEOFs in figure 5 have the characteristics of a conjugate pair, as do the next pair of EEOFs. The next four EEOFs (not shown) form two more conjugate pairs, but their interpretation is more difficult. The oscillation indicated by the first pair of EEOFs shows eastward propagation between about 75°E and 200°E (as in Plate 1d); and the time lag between maxima is 55 days. The phase speed of anomalies is 3–4 m $s^{-1}$. High variance is confined to the Indian Ocean and western Pacific (75°E–200°E). By contrast, the oscillation indicated by the second pair of EEOFs is somewhat more broadly distributed in longitude, shows no identifiable eastward or westward propagation, and the time lag between maxima is 35 days.

The time series of the coefficients of the EEOFs, or principal components (PC) (Figure 6), reveal both the intraseasonal cycles and the seasonal envelope, with smaller variance during southern winter as noted above. Spectral analysis confirms what a visual inspection suggests: The dominant spectral peak for PC1 and PC2 is at 50 days, while the dominant spectral peak for PC3 and PC4 is at 36 days. (Note that the temporal resolution of the PCs is 1 day, while the temporal resolution of the EEOFs is 5 days.) Based on the spatiotemporal structure revealed in Figure 5 and the characteristics of the time series just discussed, it seems reasonable to associate the first pair of EEOFs with the band of variance at 50–60 days and wavenumbers 1–4 in Figure 4 and to associate the second pair of EEOFs with the $k = 0$ mode at 37 days in Figure 4.

Figure 7 is a reconstruction of the longitude-time section in plate 1d using combinations of the PCs. The original longitude-time section is shown for comparison alongside reconstructions using PC 1 and 2 only, PC 3 and 4 only, and PC 1, 2, 3 and 4 combined. Figure 7 highlights the eastward moving anomalies in the original data and demonstrates how the eastward propagation is captured by the EEOFs. Most of the eastward propagation west of the dateline is picked out by EEOF 1 and 2. EEOF 3 and 4 account for less of the variance, but their inclusion increases the eastward extent of the anomalies.

**3.2.1. Relationship with other meteorological fields.**

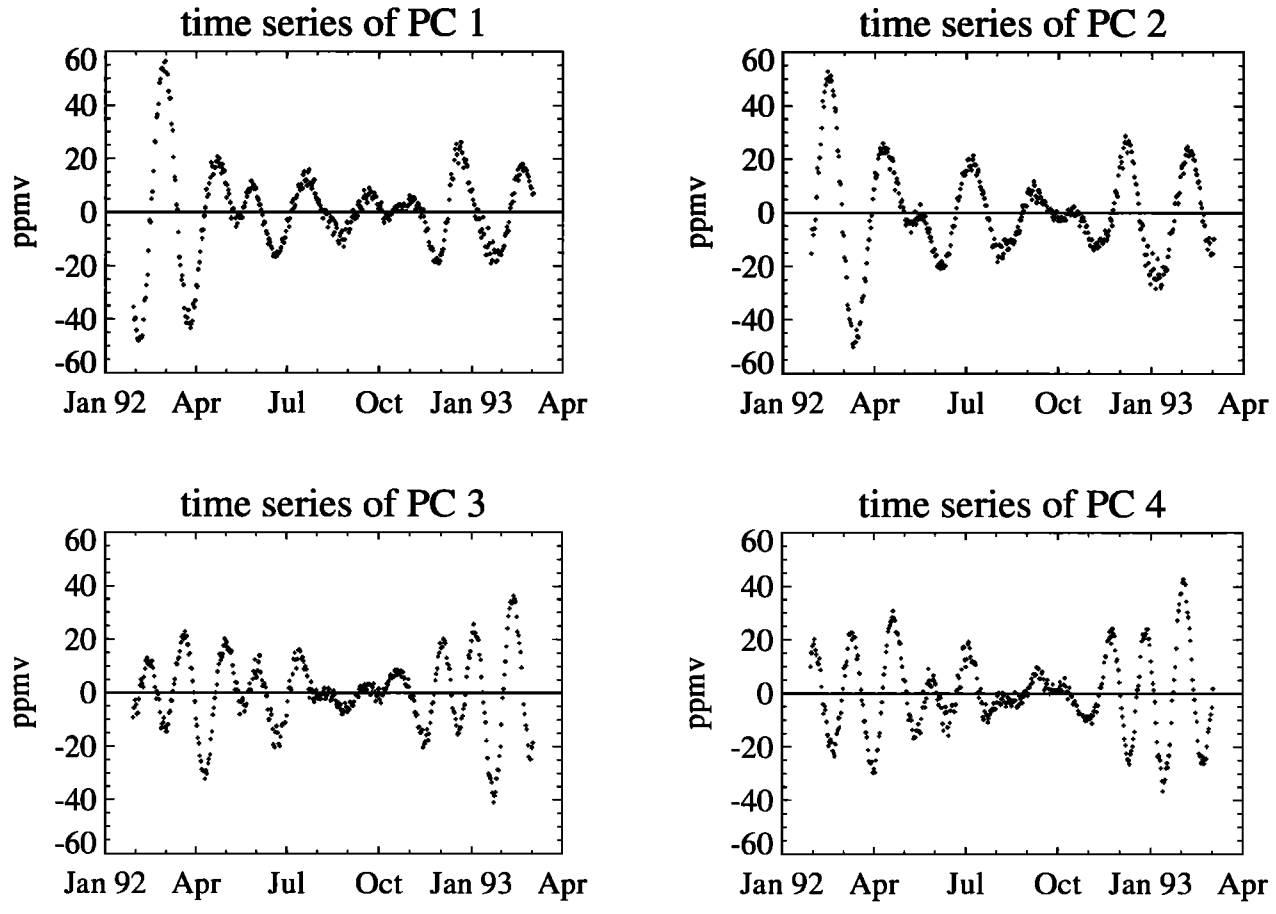


**Figure 6.** Time series of the coefficients of the EEOFs (principal components (PC)) in the previous figure.

In order to strengthen the proposed identification between the water vapor anomalies and MJO, the water vapor field is compared with vertical velocity and zonal winds obtained from ECMWF reanalysis. We examine the lifecycle of water vapor during the eastward moving event in December 1991 to February 1992 identified in section 3.2, and compare this to midtropospheric vertical velocity at 500 hPa. Both quantities are plotted as 5 day averages in Figure 8 where water vapor mixing ratios >170 ppmv are shaded in grey and upward vertical velocity less than -0.05 Pa $s^{-1}$ is colored black. The dates indicate the middle of each pentad.

From December 17-22, mixing ratios >170 ppmv are spread out in a band along the equator. Several small pockets of vertical velocity are strung out along the equator from Africa as far as 135°W and there is indication of the South Pacific Convergence Zone (SPCZ). On the December 27, the distribution of high water vapor begins to shift from Africa and the Indian Ocean toward Indonesia. Similarly, the distribution of pockets of vertical velocity has shifted from Africa and the Indian Ocean toward Indonesia. Both the SPCZ and the ITCZ are well pronounced in the vertical velocity field.

On the January 1, there is a large vertical velocity pocket over the west Pacific and a corresponding area of high mixing ratio is beginning to develop. By January 6, the moist area has moved eastward from Indonesia to become centered over the western Pacific and vertical velocity is still strong at this time. On the January 11, the pocket of vertical velocity begins to break up, but water vapor mixing ratios remain high and continue to migrate eastward and to intensify along the SPCZ. The SPCZ remains a strong characteristic in both the vertical velocity and water vapor fields until February 5, but lingers as a feature in water vapor for a further 5 days. On the February 10, the small pockets of vertical velocity have returned to Africa and the Indian Ocean and mixing ratios have begun to increase here also. Finally, water vapor disperses from the SPCZ.

This correspondence between water vapor and vertical velocity illustrates a strong relationship between high mixing ratios and convection and indicates that the convective system as a whole moves eastward rather than the water vapor being advected along at the 215 hPa level. The patterns of water vapor mixing ratio are similar to those in OLR during the MJO in March–April 1988 described by *Matthews et al.* [1996]. Both begin as a low intensity band along, and mostly south of, the equator which becomes organized over Indonesia and the west Pacific and is followed by development in a southeast direction along the SPCZ. Again, the SPCZ remains prominent in the water vapor field for longer than in OLR. *Knutson and Weickmann* [1987] noted the development of OLR from the Indian Ocean to the SPCZ. *Rui*

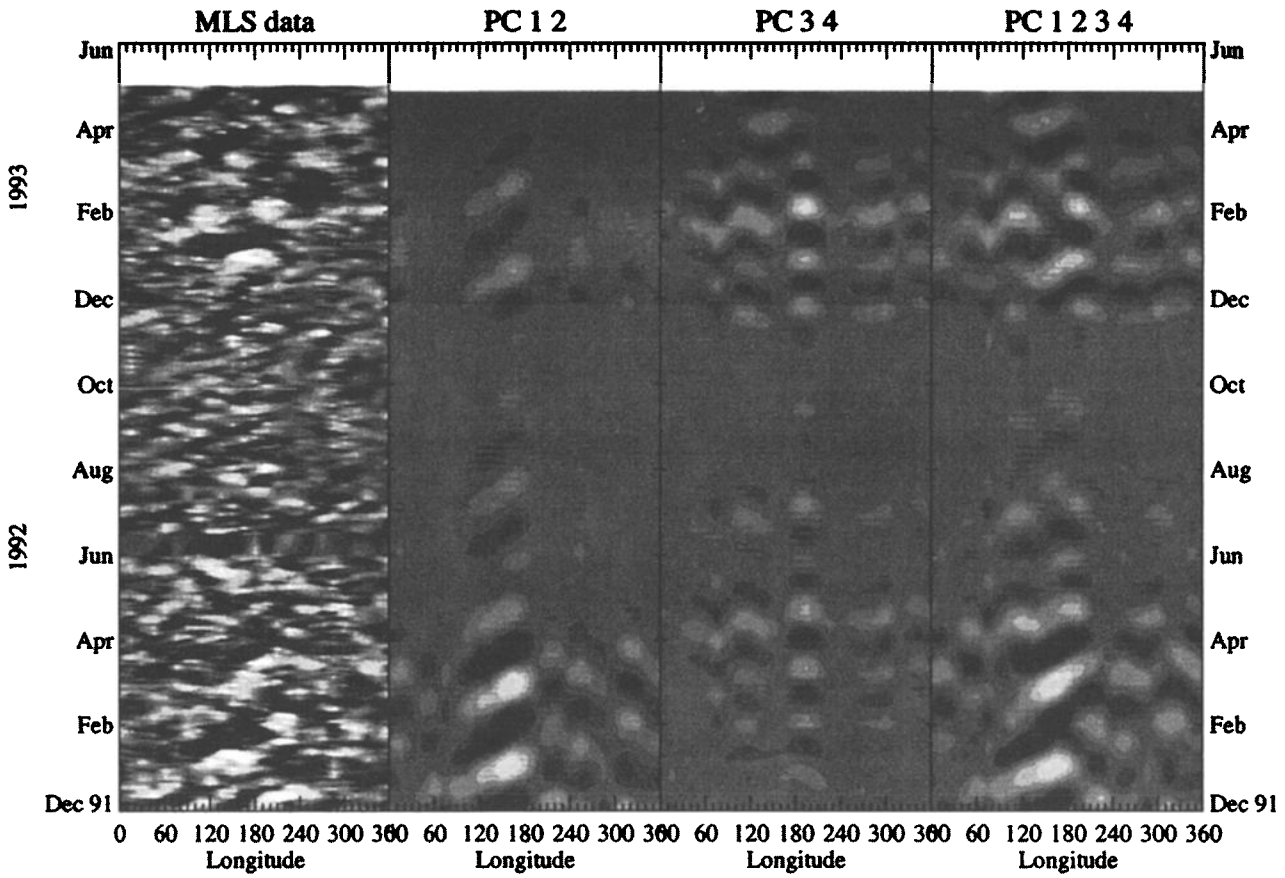


**Figure 7.** Reconstruction of the longitude-time section using combinations of the principal components (PC).

*and Wang* [1990] found that development along the SPCZ occurred in strong MJO events, and *Matthews et al.* [1996] found that enhancement or excitation of convection along the SPCZ is observed in virtually all MJOs from 1979 to 1988.

The high water vapor mixing ratios also appear to be related to westerly wind bursts in the lower troposphere. *Wang* [1988] showed that although the mean surface winds in the tropics are easterly, they are often westerly in the region where convective anomalies associated with the MJO originate. *Zhang* [1996] found that deep convection tended to occur in connection with 850 hPa westerly wind perturbations, and *Hendon and Glick* [1997] showed that westerly wind anomalies were related to enhanced evaporation. A time series of zonal winds at 850 hPa and 10°S is shown in Figure 9. Regions of westerly wind are evident during southern summer in both 1992 and 1993 and are well correlated with the eastward moving moist features in the longitude-time plot of water vapor (Plate 1d). The longitudinal extent of the westerly winds in 1992 (from 40°–200°E) corresponds well with the more evident eastward propagation in the water vapor field of this year.

In contrast to the zonal winds at 10°S, westerly wind bursts at the equator (not shown) are weaker and have a limited longitudinal extent. Similarly, *Zhang and Hendon* [1997] who also used 850 hPa zonal winds from the ECMWF analysis showed that the maximum intraseasonal variance in zonal wind was off the equator and concentrated in the western Pacific. This is an important reason for the mixing ratios being higher at 10°S than at the equator and further indication that the high mixing ratios are a result of enhanced evaporation and convection. The fact that the largest variances do not lie on the equator appears to be in conflict with those theories which attribute the MJO to moist Kelvin waves, as remarked by *Zhang and Hendon* [1997].

**3.2.2. Interannual variability.** There have been suggestions that the MJO varies in strength from year to year and that this may be related to the El Niño-Southern Oscillation phenomenon [e.g., *Lau and Chan,* 1986]. Accordingly, we have investigated the behavior of the MLS upper tropospheric humidity data for other years. There are some practical difficulties with this as data gaps prevent a detailed investigation of the southern summer months. The data gaps have increased in length as the spacecraft and instrument have aged and make later years more difficult to study. Longitude-time sections for southern summer periods are shown for 10°S in Plate 2 for all the available MLS data. Data have been treated in the same way as for Plate 1. Because there were not sufficient data for the southern summer of 1994–1995, that period is omitted.

Signs of eastward propagation are most apparent in 1991–1992 when mixing ratios between 170 and 195 ppmv reach

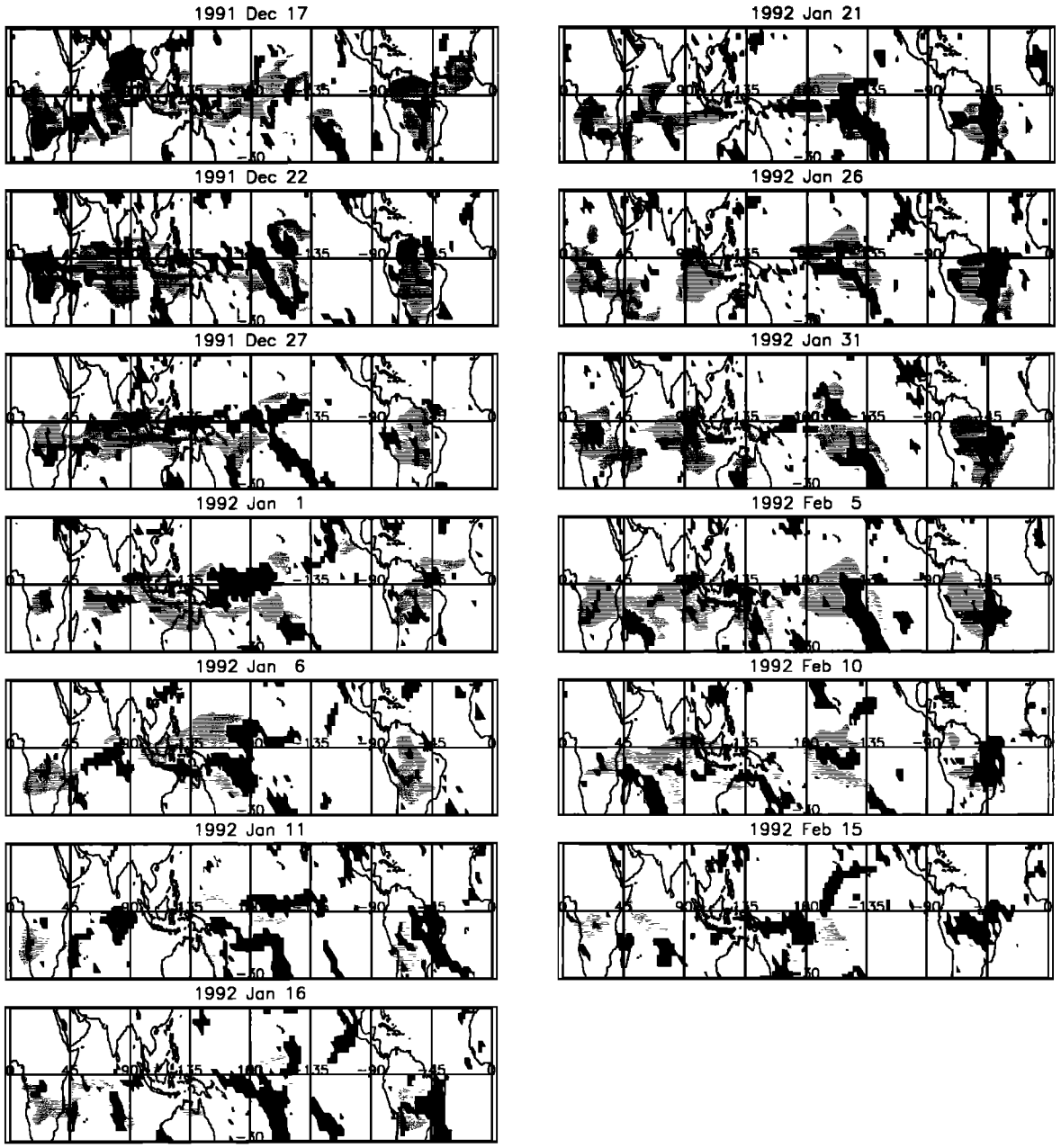


**Figure 8.** The 5 day averaged water vapor mixing ratios, at 215hPa and >170 ppmv (grey) and ECMWF vertical velocity at 500hPa and <-0.05 Pa $s^{-1}$ (black). Dates indicate the middle of the pentad.

as far as 240°E (120°W). This is further east than in any other year, and it should be noted that this was an El Niño year [*Trenberth,* 1997]. In all other years, mixing ratios >170 ppmv never extend further east than 210°E (150°W). *Knutson and Weickmann* [1987] noticed similar behavior in OLR and proposed that low sea surface temperatures or descending motion associated with the Walker circulation suppress further eastward development. Hence, the greater extent of the anomalies in 1991–1992 is probably a result of the eastward shift of convection that is a fundamental component of ENSO.

In 1992–1993 (Plate 2b), the 30-85 day filter band accounts for 52% of the variance compared with 63% in 1991–1992, and in 1992–1993 eastward movement is less evident. In the summer of 1993–1994 (Plate 2c), total variance is the same as in 1991–1992, but that associated with eastward propagation is less. In 1995–1996, a La Niña year [*Trenberth,* 1997], the lowest mixing ratios of any of the years, <70 ppmv, are reached over the eastern Pacific, and the mean and maximum mixing ratios are also lower than in other years, with the maximum mixing ratios never exceeding 245 ppmv. Although the data in 1996–1997 are sparse, mixing ratios can be seen to be as high as those in 1991–1992, and there may even be signs of eastward propagation in late February and early March. High mixing ratios do not have the same eastward extent as in 1991–1992. *Salby and*

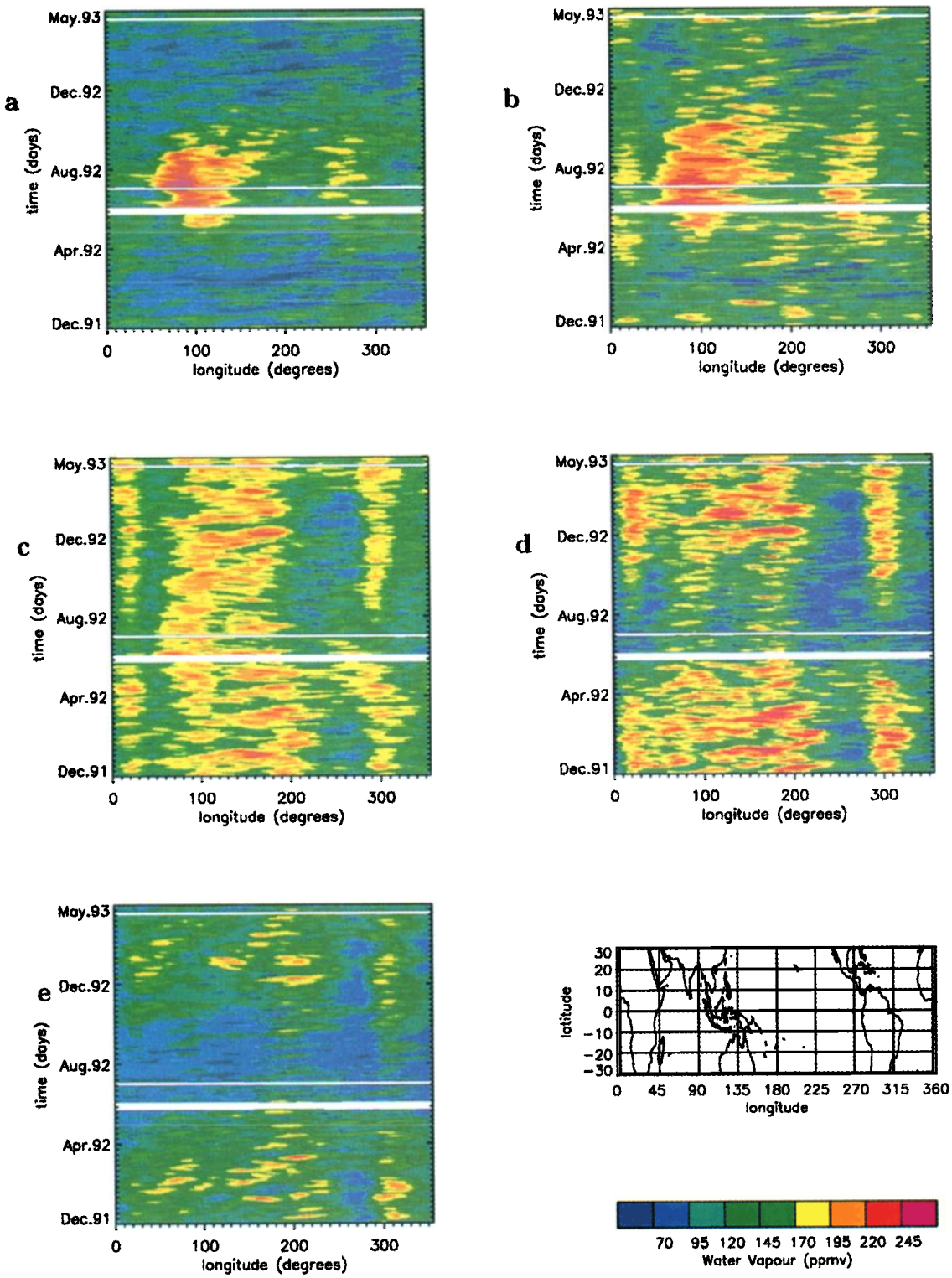


**Plate 1.** Longitude-time sections of water vapor mixing ratios (ppmv) at 215 hPa and latitudes of (a) 20°N, (b) 10°N, (c) 0°, (d) 10°S, and (e) 20°S. Data have been Kalman filtered and a mask applied to gaps of more than 3 days.

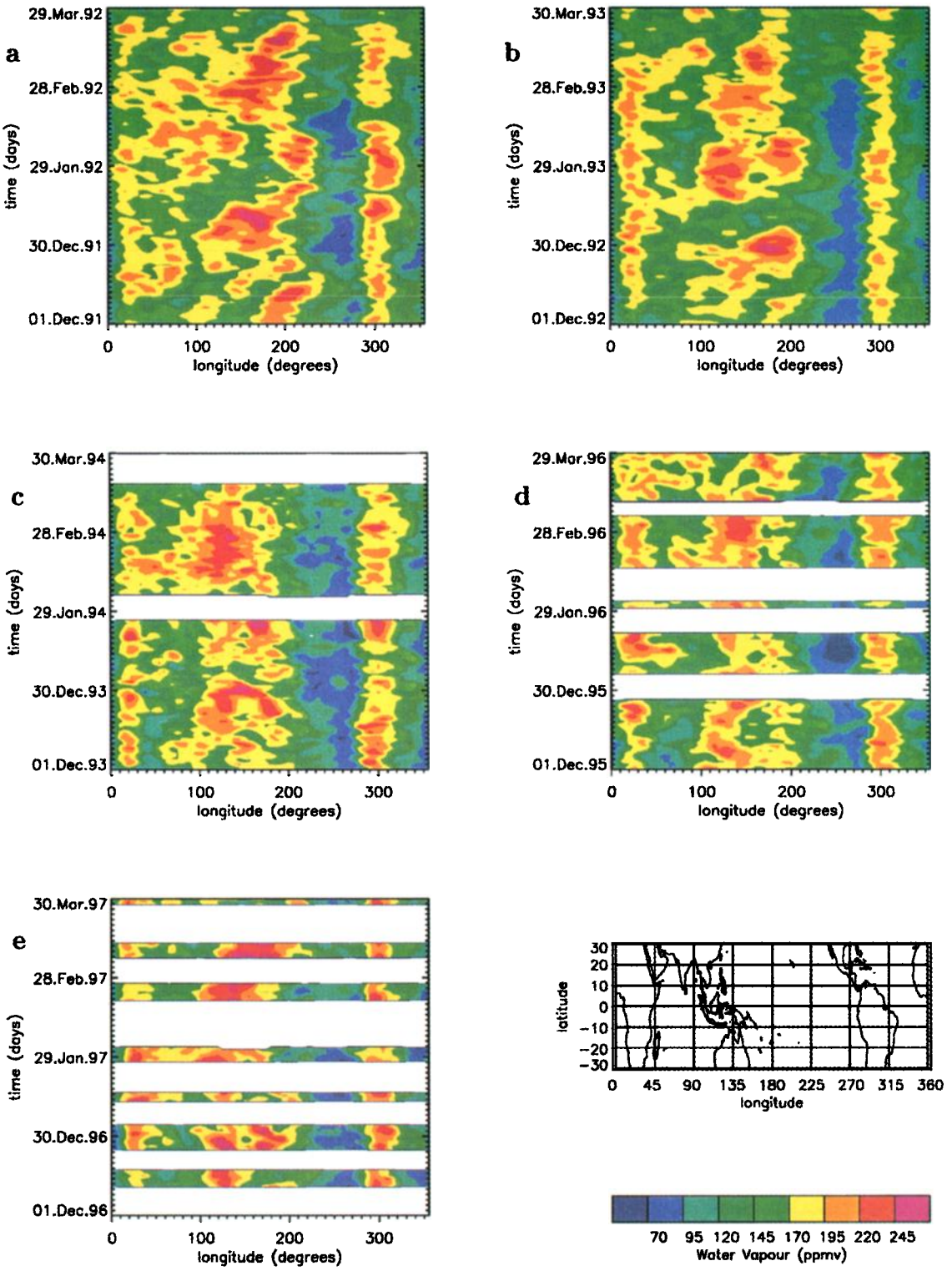


**Plate 2.** Longitude-time sections of water vapor mixing ratios (ppmv) at 215 hPa and 10°S for 120 days of southern summer from December–March in (a) 1991–1992, (b) 1992–1993, (c) 1993–1994, (d) 1995–1996, (e) 1996–1997. Data have been Kalman filtered, and a mask has been applied to gaps of more than 3 days.

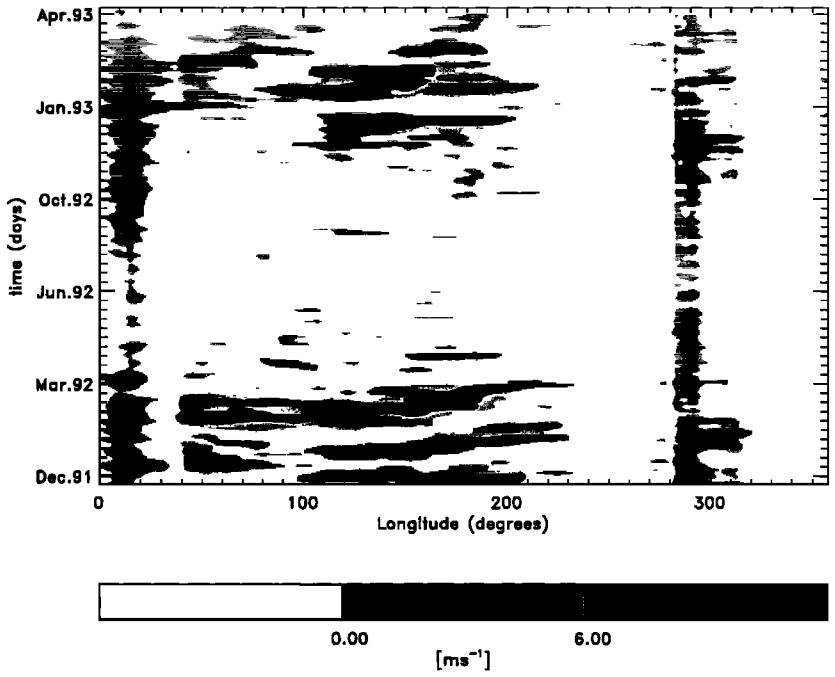


**Figure 9.** Longitude-time section of ECMWF zonal winds (m $s^{-1}$) at 10°S and 850 hPa.

*Hendon* [1994] found that the convective signal was absent during the strong ENSO cycle of 1982–1983 The relationship between the MJO and ENSO warrants further investigation.

## 4. Conclusions

We have shown that water vapor in the tropical upper troposphere varies on both annual and intraseasonal timescales. The annual cycle can be clearly seen in longitude-time sections of water vapor, but during southern hemisphere's summer, variability at intraseasonal timescales exceeds variability at the annual timescale. The annual cycle is most pronounced over the landmasses of South America and Africa, in agreement with the study by *Newell et al.* [1997]. Although the annual cycle is generally smaller over the oceans, local maxima occur in some oceanic locations, notably in regions influenced by the Asian monsoon and over Indonesia and the central Pacific.

Longitude-time sections revealed eastward moving moist anomalies that were most prominent at 10°S from December 1991 to March 1992. It is significant that this period coincides with an El Niño. The features originate in the Indian Ocean and propagate at speeds of 3-4 m $s^{-1}$ until they reach the eastern Pacific. The EEOF analysis and wave-frequency analysis reveal eastward propagating modes at 30-60 days. These spectral characteristics in space and time (Figures. 4, 5, and 6) together with the longitudinal lifecycle of the moist anomalies observed in longitude-time sections, resemble those of the MJO. We therefore identify the anomalies with the convective component of the MJO. The longitudinal extent of the intraseasonal signal was limited to the western Pacific where it dominated over the annual cycle during the time period from December 1991 to May 1993.

In addition to the eastward propagating modes interpreted as the MJO, zonally symmetric modes with periods of ~37 and 74 days have also been identified from the EEOF analysis, combined with spectral analysis of the principal components (Figures 5 and 6) and from power-spectrum analysis and wavenumber-frequency spectral analysis (Figures 3 and 4). These may be related to standing components of tropical convection which have been observed in OLR and 150 hPa divergence [e.g., *Hsu et al.*, 1990; *Zhu and Wang*, 1993; *Zhang and Hendon*, 1997].

A sequence of pentad maps showed the movement of moist anomalies from Africa across the Indian Ocean, intensification over Indonesia and the West Pacific and development along the SPCZ. The vertical velocity field has similar characteristics, lending support to our assertion that the moist anomalies at 215 hPa are associated with slowly translating convection. The origin of the moist anomalies would appear to be enhanced surface evaporation during westerly wind bursts, which were seen to be strongly correlated with water vapor and are known to play an important part in generating and maintaining the MJO.

**Acknowledgments.** The water vapor data was produced at the Jet Propulsion Laboratory, California Institute of Technology, under contract with NASA and funded through its UARS Project. The work was supported by NERC in the UK and by NASA contracts NAS1-96071 and NAS5-32862. The authors thank H.C. Pumphrey for useful discussions.

## References


Barath, F., et al., The Upper Atmosphere Research Satellite Microwave Limb Sounder Instrument, *J. Geophys. Res., 98*, 10751-10762, 1993.

Bond, S.T., The potential effect of cirrus on Microwave Limb Sounder retrievals, Ph.D. thesis, pp.161-173, Univ. of Edinburgh, Scotland, United Kingdom, 1996.

Chou, M.-D., Coolness in the tropical Pacific during an El Niño episode, *J. of Clim., 7*, 1684-1692, 1994.

Elliot, W.P. and D.J. Gaffen, On the utility of radiosonde humidity archives for climate studies, *Bull. Am. Meteorol. Soc., 72*, 1507-1520, 1991.

Elson, L.S., W.G. Read, J.W. Waters, P.W. Mote, J.S. Kinnersley, and R.S. Harwood, Space-time variations in water vapor as observed by the UARS Microwave Limb Sounder, *J. Geophys. Res., 101*, 9001–9015, 1996.

Gilman, D.L., F.J. Fuglister and J.M. Mitchell Jr., On the power spectrum of red noise, *J. Atmos. Sci., 20*, 182-184, 1963.

Hendon, H.H. and J. Glick, Intraseasonal air-sea interaction in the tropical Indian and Pacific oceans, *J. of Clim., 10*, 647-661, 1997.

Houghton, J.T., G.J. Jenkins, and J.J. Ephraumus, *Climate Change: The IPCC Scientific Assessment*, Cambridge Univ. Press, New York, 1990.

Hsu, H-H., B.J. Hoskins and F-F. Jin, The 1985/86 intraseasonal oscillation and the role of the extratropics, *J. Atmos. Sci., 47*, 823-839, 1990.

Jackson, D.R., R.S. Harwood, and E. Renshaw, Tests of a scheme for regression retrieval and space-time interpolation of stratospheric temperature from satellite measurements, *Q. J. R. Meteorol. Soc., 116*, 1449-1470, 1990.

Jones, R.L. and J.F.B. Mitchell, Is water vapor understood?, *Nature, 353*, 212, 1991.

Kiladis, G.N. and K.M. Weickmann, Circulation anomalies associated with tropical convection during northern winter, *Mon. Weather Rev., 120*, 1900-1923, 1992.

Knutson, T.R., and K.M. Weickmann, 30-60 day atmospheric oscillations: Composite lifecycles of convection and circulation anomalies, *Mon. Weather Rev., 115*, 1407-1437, 1987.

Lau, K.M. and P.H. Chan, The 40-50 day oscillation and ENSO: A new perspective, *Bull. Am. Meteorol. Soc., 67*, 533-534, 1986.

Lindzen, R.S., Some coolness concerning global warming, *Bull. Am. Meteorol. Soc., 71*, 288-299, 1990.

Madden, R.A. and P.R. Julian, Detection of a 40-50 day oscillation in the zonal wind in the tropical Pacific, *J. Atmos. Sci., 28*, 702-708, 1971.

Matthews, A.J., B.J. Hoskins, J.M. Slingo, and M. Blackburn, Development of convection along the SPCZ within a Madden-Julian oscillation, *Q. J. R. Meteorol. Soc., 122*, 669-688, 1996.

Newell, R.E., Y. Zhu, W.G. Read, and J.W. Waters, Relationship between tropical upper tropospheric moisture and eastern tropical Pacific sea surface temperature at seasonal and interannual timescales, *Geophys. Res. Lett., 24*, 25-28, 1997.

Newell, R.E., Y. Zhu, E.V. Browell, W.G. Read, and J.W. Waters, Walker circulation and tropical upper tropospheric water vapor, *J. Geophys. Res., 101*, 1961-1974, 1996.

Philander, S.G.H., D. Gu, D. Halpern, G. Lambert, N.-C. Lau T. Li, and R.C. Pacanowski, Why the ITCZ is mostly north of the equator, *J. of Clim., 9*, 2958-2972, 1996.

Read, W.G., J.W. Waters, D.A. Flower, L. Froidevaux, R.F. Jarnot, D.L. Hartmann, R.S. Harwood, and R.B. Rood, Upper tropospheric water vapor from UARS MLS, *Bull. Am. Meteorol. Soc., 76*, 2381-2389, 1995.

Reber, C.A., The upper atmosphere research satellite (UARS), *Geophys. Res. Lett., 20*, 1215-1218, 1993.

Rui, H., and B. Wang, Development characteristics and dynamic structure of tropical intraseasonal convection anomalies, *J. Atmos. Sci., 47*, 357-379, 1990.

Salathé, E.P. and D. Chesters, Variability of moisture in the upper troposphere as inferred from TOVS satellite observations and the ECMWF model analysis in 1989, *J. of Clim.*, 8, 120-132, 1995.

Salby, M.L., and H.H. Hendon, Intraseasonal behaviour of clouds, temperature and motion in the tropics, *J. Atmos. Sci., 51*, 2207-2224, 1994.

Schmetz, J., and O.M. Turpeinen, Estimation of the upper tropospheric humidity field from METEOSAT water vapour image data *J. Appl. Meteorol.*, 27, pp 889-899, 1988.

Soden, B.J., Variations in the tropical greenhouse effect during El Niño, *J. of Clim., 10*, 1050-1055, 1997.

Soden, B.J. and F.P. Bretherton, Upper-tropospheric relative humidity from the GOES 6.7 $\mu$m channel: Method and climatology for July 1987, *J. Geophys. Res., 98*, 16669-16688, 1993.

Soden, B.J., and J.R. Lanzante, An assessment of satellite and radiosonde climatologies of upper-tropospheric water vapor, *J. of Clim., 9*, 1235-1250, 1996.

Spencer, R.W., and W.D. Braswell, How dry is the tropical free troposphere? Implications for global warming theory, *Bull. Am. Meteorol. Soc., 78*, 1097-1106, 1997.

Trenberth, K.E., The definition of El Niño, *Bull. Am. Meteorol. Soc., 78*, 2771–2777, 1997.

Wang, B., Reply to comment by B. Wang on "An air-sea interaction model of intraseasonal oscillations in the tropics", *J. Atmos. Sci., 44*, 3521-3525, 1988.

Wang, R., K. Fraedrich, and S. Pawson, Phase-space characteristics of the tropical stratospheric quasi-biennial oscillation, *J. Atmos. Sci., 52*, 4482–4500, 1995.

Waters, J.W., Microwave Limb Sounding, in *Atmospheric Remote Sensing by Microwave Radiometry,* edited by M.A. Janssen, 383-496, John Wiley, New York, 1993.

Weare, B.C., and J.S. Nasstrom, Examples of extended empirical orthogonal function analysis, *Mon. Weather Rev., 110*, 481–485, 1982.

Zhang, C., Atmospheric intraseasonal variability at the surface in the tropical western Pacific Ocean, *J. Atmos. Sci., 53*, 739-756, 1996.

Zhang, C., and H.H. Hendon, Propagating and standing components of the intraseasonal oscillation in tropical convection, *J. Atmos. Sci., 54*, 741-752, 1997.

Zhu, B., and B. Wang, The 30-60 day convection seesaw between the tropical Indian and western Pacific Oceans, *J. Atmos. Sci., 50*, 184-199, 1993.



H. L. Clark and R. S. Harwood, Department of Meteorology, University of Edinburgh, West Mains Road, Edinburgh, U.K. EH8 3JZ. (e-mail: H.Clark@ed.ac.uk; r.harwood@ed.ac.uk

P. W. Mote, Northwest Research Associates, P.O. Box 3027, Bellevue, WA 98009. (e-mail: mote@nwra.com)

W. G. Read, Jet Propulsion Laboratory, 4800 Oak Grove Drive, Pasadena, CA, 91109-8099. (e-mail: bill@mls.jpl.nasa.gov)


(Received January 28, 1998; revised July 17, 1998; accepted August 14, 1998.)